

# Intelligent Processing Technology for Time-series Archived Historical Aerial Photos Based on Cloud Control Photogrammetry

Xiaokun Zhu,<sup>1\*</sup> Chen Liang,<sup>1</sup> Huimin Tian,<sup>1</sup> Mingce Xu,<sup>2</sup> and Yutao Guo<sup>1</sup>

<sup>1</sup>Bigdata Centre, Beijing Institute of Surveying and Mapping,  
No. 60, Nanlishi Road, Xicheng District, Beijing 100045, P.R. China

<sup>2</sup>Beijing SmartSpatio Technology,  
Da Cheng Era Center, No. 6, Da Cheng Road, Fengtai District, Beijing 100141, P.R. China

(Received August 9, 2024; accepted March 28, 2025)

**Keywords:** cloud control photogrammetry, archived aerial photo, time series, intelligent processing, LiDAR

For the historical archives of time-series image resources from different sensors, the original photos often go unnoticed because of the lack of ground control points (GCPs). In this paper, we propose a GCP-free intelligent processing methodology for time-series archived historical aerial photos, which is based on cloud control photogrammetry and leverages airborne light detection and ranging (LiDAR) point cloud data. The key technologies discussed include the acquisition and accuracy evaluation of reference data, image matching, and aerial triangulation for subsequent three-dimensional (3D) modeling utilization. To validate our proposed method, we conducted experiments within the Fourth Ring Road area of Beijing's Plain District, covering approximately 320 km<sup>2</sup>, using LiDAR data, the digital aerial photos obtained by AMC in 2017, the digital aerial photos obtained by UCXP in 2015, and the aerial films obtained by RC-10 in 1975–1990. On the basis of experimental results, it was concluded that a robust network of cloud control points with an interval of at least 1000 pixels could be established to replace traditional field GCPs, enhancing both the effectiveness and reliability of automated processing. Furthermore, experimental results demonstrated that this method allowed for the relaxation of orientation accuracy requirements for cloud control points from 0.35 to 0.6 pixels while maintaining the same level of accuracy. Even in cases where significant differences exist between the reference data and the archived photos, effective control can still be achieved by cloud control photogrammetry, with a threshold for eliminating gross errors set at 2–3 times the root mean square error.

## 1. Introduction

Conventional methods for acquiring ground control points (GCPs) typically involve fieldwork that requires an extended timeframe to achieve a complete coverage of the research area.<sup>(1)</sup> Zhang and Tao from Wuhan University introduced the concept of cloud control

---

\*Corresponding author: e-mail: [zhuxk@radi.ac.cn](mailto:zhuxk@radi.ac.cn)  
<https://doi.org/10.18494/SAM5302>

photogrammetry,<sup>(2)</sup> which leverages image-matching technology to automatically derive a substantial number of high-density control points from referenced geographic information data instead of GCPs. This process is termed cloud control because it generates exceptionally dense point clouds. The sources of cloud control data for this approach include a variety of datasets, such as satellite laser altimetry data, light detection and ranging (LiDAR) data from different sensors including airborne and mobile vehicles, aerotriangulation results, digital orthophoto map (DOM), digital elevation model (DEM), and digital line graphic (DLG) data. Currently, DOM- and DEM-based cloud control photogrammetry finds widespread applications in the unattended intelligent processing of satellite remote sensing imagery, including satellite calibration, digital orthophoto production, the three-dimensional (3D) modeling of real scenes in China, and mapping uninhabited regions.<sup>(3–6)</sup> In contrast, the utilization of aerotriangulation parameters and LiDAR data within cloud control photogrammetry is infrequent but holds a significant potential value.

LiDAR data has gradually become a new standard geospatial information product. With its high density, uniform distribution, and high absolute accuracy (up to 10 cm for both plane and elevation), as well as consistent relative accuracy, the point cloud acquired by LiDAR sensors can be utilized as high-precision geometric control information to achieve large-scale aerial photogrammetry without field GCPs.<sup>(7)</sup> Many countries around the world, including Canada, Denmark, Finland, the Netherlands, Poland, Spain, Sweden, Switzerland, the United States, the United Kingdom, and New Zealand have established national LiDAR datasets as a basic data framework.<sup>(8)</sup> From 2015 to 2017, LiDAR data acquired for DEM production could be explored as archived aerial data processing sources for cloud control photogrammetry.

In the historical archives of time-series image resources acquired from different sensors, traditional DOM products are preserved and widely used. However, original aerial photos often go unnoticed because of the lack of GCPs, their large quantity, and inconsistent coordinate systems.<sup>(9)</sup> In recent years, there has been a growing recognition of the importance of archived historical aerial photographs as a means of restoring historical 3D models.<sup>(10)</sup> Therefore, in this study, we attempt to develop an intelligent processing methodology that is free of GCPs for time-series archived historical aerial photos, which is based on cloud control photogrammetry and leveraging LiDAR point cloud data. The key technologies discussed include the acquisition and accuracy evaluation of reference data, image matching, and aerial triangulation. This methodology aims to provide a reference for subsequent 3D modeling utilization.

## **2. Methodology**

### **2.1 Workflow**

The workflow for processing time-series archived historical aerial photos based on cloud control photogrammetry is illustrated in Fig. 1. It primarily consists of five components: the evaluation and selection of cloud control sources, the organization of cloud control sources, cloud control aerial triangulation with LiDAR and reference data, cloud control aerial triangulation using digital control photos (DCPs) for archived photo processing, and time-series photogrammetry result output.

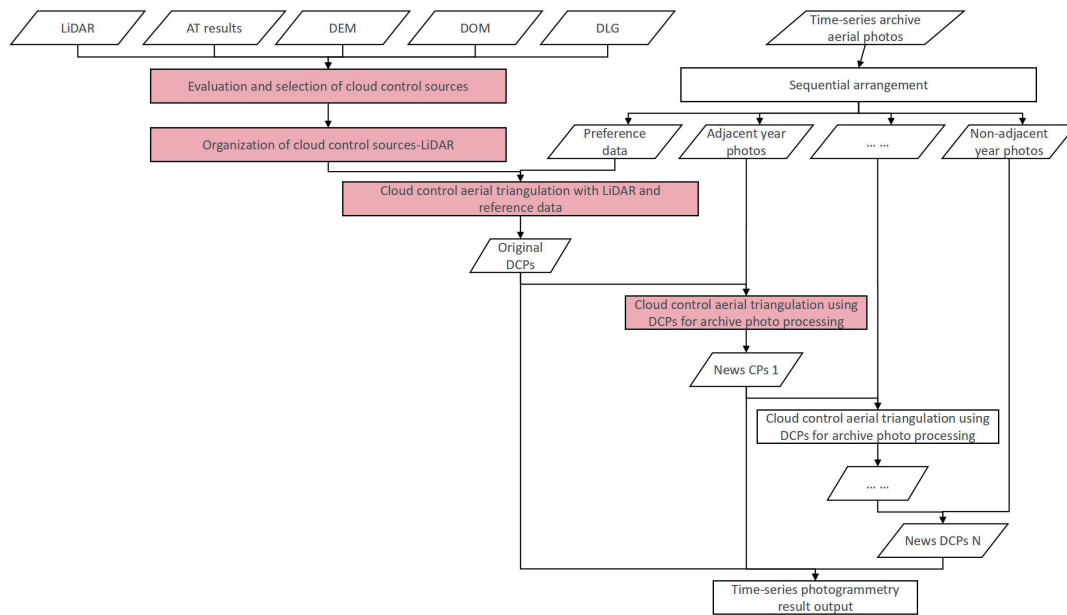


Fig. 1. (Color online) Workflow chart.

## 2.2 Methods

### (1) Cloud control source evaluation and selection

Considering the density of available control points and cloud control accuracy, the priority sequence for selecting cloud control sources is as follows: LiDAR data from airborne sensors, aerotriangulation results, DOM with DEM, and DLG with DEM. It is preferable to choose LiDAR data as the cloud control source after removing noise and correcting intertrip systematic errors,<sup>(11)</sup> ensuring that its coverage contains or matches that of the processed photos. The accuracy of the control source should exceed the result accuracy requirements of the data to be processed. Considering matching errors, it is recommended that the data acquisition times be as close as possible to minimize changes in the entire test area to less than 50%, such as the same season, similar solar elevation angles, and so on.

### (2) Organization of cloud control sources

The organization of the cloud control sources should follow a unified format and content to facilitate automated processing in later stages. In cases where a single control source is insufficient, multiple control sources can be utilized. Boundary errors must not exceed twice the error margin in the results. Metadata information for various control sources, including coordinate projection, point cloud density, spatial resolution, and data acquisition time, should be compiled.

### (3) Cloud control aerial triangulation with LiDAR and reference data

In the selection of reference data, resolution and acquisition time are considered, with preference given to aerial photos that closely match the average point density and the timing of LiDAR data acquisition for the subsequent processing of historical aerial photos. Cloud

control points are matched between LiDAR and reference data, ensuring an even distribution within the block with an average interval of less than 1000 pixels and a root mean square adjustment of less than 1 pixel. Following block adjustment, DCPs<sup>(12)</sup> are generated from original photos, orientation parameters, and coordinates of matching cloud control points.

The process of cloud control aerial triangulation based on LiDAR point cloud and reference data is illustrated below in Fig. 2.

Positioning and orientation system (POS)-assisted aerial triangulation (AT) technology is utilized for preprocessing the reference images and extracting sparse feature points and feature lines.<sup>(13)</sup> Subsequently, point cloud segmentation technology is employed to process LiDAR points to obtain segmentation surfaces. Following this, the iterative closest point (ICP)<sup>(14)</sup> or iterative closest line (ICL)<sup>(15)</sup> algorithm is applied iteratively to optimize image orientation parameters using the distance least squares method. On the basis of LiDAR point-constrained block adjustment, the object and image coordinates of the cloud control points are updated. Throughout this process, the adaptive determination of weight for LiDAR points and surface feature control information is based on local point coplanarity.

Proposed by Besl and McKay in 1992,<sup>(14)</sup> the iterative closest point (ICP) algorithm is a classical geometric registration method used in cloud control photogrammetry. Its enhanced version is widely applied directly or indirectly to the geometric registration of images to 3D point clouds. The primary objective of the ICP algorithm is to address the issue of inconsistent coordinate systems between two distinct point clouds, aiming to merge them into a unified coordinate system. The ICP algorithm imposes certain requirements on the initial alignment accuracy of two sets of point clouds. In this study, we employ the principle of point-to-plane nearest distance, as illustrated in Fig. 3. For any sparse feature point  $P_i = (p_{ix}, p_{iy}, p_{iz}, 1)^T$  with

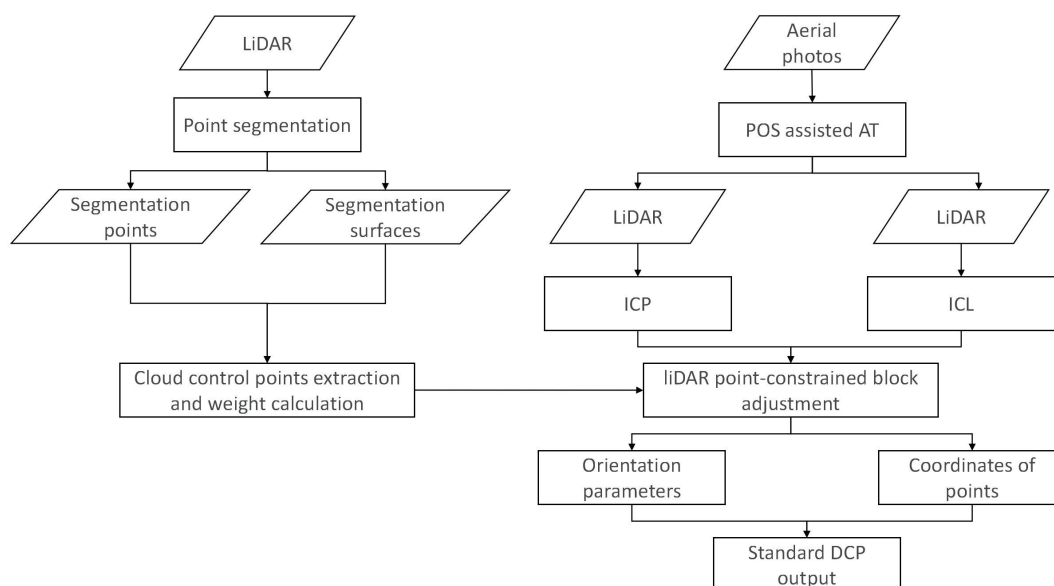


Fig. 2. Process of cloud control aerial triangulation with LiDAR point cloud and reference data.

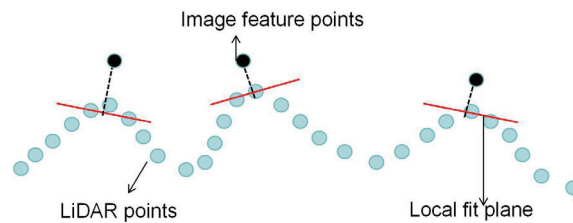


Fig. 3. (Color online) Point-to-plane distance in ICP algorithm.

$p_{ix}$ ,  $p_{iy}$ ,  $p_{iz}$  representing the 3D coordinate values of the point  $P_i$ , a spatial plane  $a_i x + b_i y + c_i z + d_i = 0$  (depicted as the red line segment in Fig. 3) is obtained by fitting it to the nearest point set in the LiDAR point cloud. The parameters of the plane are denoted as  $\mathbf{Pl}_i(a_i, b_i, c_i, d_i)$ , and its “control point” in the LiDAR point cloud refers to its foot point on the fitting plane.

The objective of the ICP algorithm is to determine the optimal transformation matrix  $\mathbf{M}_O$  that minimizes  $E(\mathbf{M}_O)$ :

$$E(\mathbf{M}_O) = \sum_{i=1}^{n_p} dis^2(\mathbf{M}_O P_i, \mathbf{Pl}_i). \quad (1)$$

Here,  $dis(\cdot)$  represents the calculation function for determining the spatial point and surface distance.  $\mathbf{M}_O$  denotes the  $4 \times 4$  spatial similarity transformation matrix that maps image sparse feature points to LiDAR point clouds, and  $n_p$  indicates the total number of points involved. The minimization problem described by this equation can be effectively addressed through nonlinear least squares optimization. Upon obtaining the optimal matrix, it can be utilized to transform the projection matrices of all images (comprising internal and external orientation parameters, excluding camera distortion factors).

LiDAR control surface features are interpolated from the LiDAR point cloud using the ICP algorithm and then integrated into the self-checking adjustment of the area network as a constraint to solve for camera distortion parameters, image internal orientation elements, and external orientation elements. At a local level, this optimization could effectively mitigate local distortions in the image area network caused by camera distortion, inconsistent image connection strength, and resulting error accumulation.

#### (4) Cloud control aerial triangulation using DCPs for archived photo processing

On the basis of the generated DCPs, historical image aerial triangulation for cloud control is re-conducted. Image registration techniques such as the scale-invariant feature transform (SIFT) or fast point feature histogram (FPFH) algorithm<sup>(16,17)</sup> are primarily utilized to match cloud control points between DCPs and archived photos. For archived images with POS information, direct utilization for registration is possible; however, in cases where POS image data is unavailable, geodetic coordinates of each line’s start and end need to be provided first, and the initial geodetic coordinates of intermediate photos can be automatically calculated

from overlap degrees. Time-series archived photos can undergo iterative processing, whereby those processed by cloud control photogrammetry with original DCPs are selected as new DCPs for subsequent photo processing; all DCPs should be standardized and exported for archiving purposes.

(5) Time-series photogrammetry result output

Time-series DCPs are generated from the cloud control aerial triangulation mentioned above, enabling the production of traditional DOM, DEM, DLG products and real-scene 3D models<sup>(18)</sup> with temporal information, which can be utilized for historical change analysis.

### 3. Experiment

#### 3.1 Experimental area

To validate the aforementioned method, experiments were conducted within the Fourth Ring Road area of Beijing's Plain District, which spans approximately 320 km<sup>2</sup>.

#### 3.2 Data sources

(1) Reference LiDAR data

LiDAR point cloud data, acquired using Optech equipment in 2017, had a point cloud density of 6–10 points per square meter.

(2) Reference oblique photos

The 86402 oblique photos captured by AMC, including images from five lenses, with a ground sample distance (GSD) of 0.05 m, were all captured in 2017.

(3) Checkpoints

Fifty field points were obtained through RTK measurements with an RMS of 5 cm.

(4) Time-series archived aerial photos

Digital aerial photos were obtained by UCXP in 2015 with a GSD of 0.2 m. Aerial films were obtained by RC-10 in 1975–1990 with a GSD ranging from 0.07 to 0.5 m.

#### 3.3 Results and Discussion

(1) The LiDAR data from 2017 was chosen as the reference data source, and the point cloud data underwent de-noising to eliminate noise points and mobile ground object points, as well as correction for system errors. Following the correction process, the accuracy was assessed using checkpoints, revealing an elevation error of  $\pm 0.14$  m. The results were based on the China Geodetic Coordinate System 2000 (CGCS2000) within a 1 km x 1 km block storage.

(2) Aerial triangulation for cloud control was carried out using the LiDAR point cloud and nonsynchronous oblique photos acquired in 2017. The interval of matched cloud control points was set at 250 pixels, with an adjustment RMS error of 0.6 pixels. Fifty checkpoints were utilized to verify that the inspection accuracy meets the mapping requirements for a scale of 1:500, with a planimetric accuracy of  $\pm 0.19$  m and an elevation accuracy of  $\pm 0.24$  m.

Following the block adjustment, the reference DCPs were generated from the original oblique photos, orientation parameters, and coordinates of the matching cloud control points.

- (3) Aerial triangulation or cloud control was carried out using reference GCPs and archived photos, which included the 2015 digital aerial and 1975–1990 RC-10 scanned photos. Despite a change of more than 50% between the RC-10 photos and those from 2017, it was still possible to align them with the main road network. The statistical error results indicate that the accuracy of the checkpoints meets mapping standards for both planimetry ( $\pm 1.5$  m) and elevation ( $\pm 0.44$  m) at a scale of 1:5000 for the photos with a resolution of 0.5m.
- (4) From the results of cloud control aerial triangulation conducted in 1975–1990, 2015, and 2017, a time-series real-scene 3D model can be effectively generated using Context Capture tools. The 3D modeling results for the Tonghui River section and Forbidden City are respectively presented in Figs. 4 and 5.



Fig. 4. (Color online) 3D modeling results for Tonghui River section of Grand Canal in (a) 1975 and (b) 2015.



Fig. 5. (Color online) 3D modeling results for Forbidden City in (a) 1990 and (b) 2017.

## 4. Conclusions

In this paper, an intelligent processing technology for time-series archived historical aerial photos based on cloud control photogrammetry is proposed. From the experimental results, the following conclusions were drawn:

This approach enhances the effectiveness and reliability of automated processing. Compared with the traditional GCP controlled method, it acquires a larger number of GCPs. By utilizing cloud control photogrammetry, we can establish a robust network of cloud control points with an interval of at least 1000 pixels utilizing both LiDAR and reference data, thereby replacing traditional field GCPs. Additionally, the experimental results demonstrate that this method allows for the relaxation of orientation accuracy requirements for cloud control points from 0.35 to 0.6 pixels while achieving the same level of accuracy.

Time-series archived photos can be iteratively processed, whereby those processed by cloud control photogrammetry with original DCPs are selected as new DCPs for subsequent photo processing. To ensure accuracy, the original DCPs were typically selected from those with the highest resolution and processed using LiDAR point cloud data. All the DCPs can serve as a novel form of output data that is readily reusable in the future.

For the aforementioned method, as the time interval between the image to be processed and the reference image increases, there are corresponding increases in the occurrence of changes and automatic matching point errors, thereby affecting the method's usability. From the experimental results, when significant changes occurred in the images between 1990 and 2015, more than 50% of the survey areas did not align with the image control points. By setting the threshold for eliminating gross errors at 2–3 times the standard value, it was possible to align them with the main road network, facilitating cloud control photogrammetry for long-period archived image data without the need for field GCPs.

## Acknowledgments

This work was supported by Ang Li at the Center for the Utilization of Surveying and Mapping Data Archive, Beijing Institute of Surveying and Mapping, for the provision of historical aerial photo support and Pengjie Tao in Wuhan University for the tools of cloud control photogrammetry. This work was supported by the Beijing Municipal Science & Technology Commission Project "Research and Demonstration Application of Key Technologies for Enhancing Resilience Spatial Planning in Beijing's Rainstorm Disaster Prevention and Mitigation" (Z241100009124013).

## References

- 1 Z. Zhang, J. Zhang, and L. Zhang: *J. Wuhan Univ. Surv. Mapp.* **25** (2000) 7. <https://doi.org/10.3969/j.issn.1671-8860.2000.01.002>
- 2 Z. Zhang and P. Tao: *Acta Geod. Cartogr. Sin.* **46** (2017) 1238. <https://doi.org/10.11947/j.AGCS.2017.20170337>
- 3 B. Yang, Y. Pi, X. Li, and Y. Yang: *ISPRS J. Photogramm. Remote Sens.* **162** (2020) 173. <https://doi.org/10.1016/j.isprsjprs.2020.02.015>
- 4 H. Cao, P. Tao, H. Li, and J. Shi: *ISPRS J. Photogramm. Remote Sens.* **156** (2019) 169. <https://doi.org/10.1016/j.isprsjprs.2019.08.011>

- 5 Y. Sun, L. Zhang, B. Xu, and Y. Zhang: J. Remote Sens. **23** (2019) 205. <https://doi.org/10.11834/jrs.20198067>
- 6 M. Wang, B. Yang, D. Li, J. Gong, and Y. Pi: Geom.: Geom. Inf. Sci. Wuhan Univ. **42** (2017) 427. <https://doi.org/10.13203/j.whugis20160534>
- 7 X. Xiong: Registration of airborne LiDAR point cloud and aerial images using multi-features. (Wuhan University,Wuhan, 2014). Ph.D. dissertation.
- 8 J. Zhang, X. Lin, and X. Liang: Acta Geod. Cartogr. Sin. **46** (2017) 1460. <https://doi.org/10.11947/j.AGCS.2017.20170345>
- 9 B. Xu: Research on the key techniques for building roof top reconstruction from aerial LiDAR pointclouds. (Wuhan University,Wuhan, 2017). Ph.D. dissertation.
- 10 B. Wei, N. Li, S. Ni, Y. Zhang, Y. Wang, C. Pan, X. Tang, F. Yang, and R. Ding: A 3D reconstruction method for historical film aerial images:CN202111255960.9 (2024-07-31).
- 11 N. C. May and C. K. Toth: Int. Arch. Photogramm. Remote Sens. Spatial Inf. Sci. **36** (2007) 107.
- 12 Z. Zhang, Y. Duan, and P. Tao: Geom. Inf. Sci. Wuhan Univ. **48** (2023) 1715. <https://doi.org/10.13203/j.whugis20230373>
- 13 X. Yuan, Y. Gao, and X. Zou: Geom. Inf. Sci. Wuhan Univ. **37** (2012) 1289. <https://doi.org/10.13203/j.whugis2012.11.014>
- 14 P. J. Besl and N. D. McKay: IEEE Trans. Pattern Anal. Mach. Intell. **14** (1992) 239. <https://doi.org/10.1117/12.57955>
- 15 A. Habib, M. Ghanma, M. Morgan, and R. Ai-Ruzouq: Photogramm. Eng. Remote Sens. **71** (2005) 600. <https://doi.org/10.14358/pers.71.6.699>
- 16 D. G. Lowe: Int. J. Comput. Vis. **60** (2004) 91. <https://doi.org/10.1023/b:visi.0000029664.99615.94>
- 17 R. B. Rusu, N. Blodow, M. Beetz: Proceedings of IEEE Int. Conf. Robotics and Automation. Kobe: IEEE, (2009) 3212. <https://doi.org/10.1109/robot.2009.5152473>
- 18 X. Zhu, G. Pang, and C. Chen: Int. Arch. Photogramm. Remote Sens. Spatial Inf. Sci. **43** (2020) 555. <https://doi.org/10.5194/isprs-archives-XLIII-B2-2020-555-2020>

## About the Authors



**Xiaokun Zhu** received her M.S. degree from Wuhan University, China, in 2005 and her Ph.D. degree from the Aerospace Information Research Institute, Chinese Academy of Science, China, in 2019. From 2005 to 2019, she was employed at the Beijing Institute of Surveying and Mapping as an engineer. Since 2020, she has been a senior engineer and her research interests are in photogrammetry and remote sensing for urban planning applications. ([zhuxk@radi.ac.cn](mailto:zhuxk@radi.ac.cn))



**Chen Liang** received his B.S. and Ph.D. degrees from Wuhan University, China, in 2012 and 2019, respectively. From 2019 to 2021, he was a lecturer at Pingdingshan University, China. From 2021 to 2023, he worked as a postdoctoral fellow at Beijing Normal University. Since 2023, he has been a senior engineer at the Beijing Institute of Surveying and Mapping. His research interests are in deep learning and geographic intelligent analysis. ([chenliang90210@whu.edu.cn](mailto:chenliang90210@whu.edu.cn))



**Huimin Tian** received her M.S. degree from China University of Mining and Technology (Beijing) in 2020. Since 2020, she has been working at the Beijing Institute of Surveying and Mapping, and since 2022, she has been an engineer. Her research interest is in urban spatial analysis. ([tianhuimin\\_0123@163.com](mailto:tianhuimin_0123@163.com))



**Mingce Xu** received his B.S. degree from Anhui Science and Technology University, China, in 2005 and his M.S. degree from the East China Normal University, China, in 2008. From 2008 to 2011, he was a technical manager at SuperMap Software Co., Ltd., China. Since 2012, he has been a founding president at SmartSpatio Inc. His research interests are in PRS, RS, AI, UAS, and sensors. ([xumingce@qq.com](mailto:xumingce@qq.com))



**Yutao Guo** received her B.S. degree from Beijing Union University, China, in 2020. Since 2020, she has been an engineer. Her research interest is in urban spatial analysis with GIS. ([guoyutao@bism.cn](mailto:guoyutao@bism.cn))